Journal of Thermal Analysis and Calorimetry (2023) 148:13003–13009
https://doi.org/10.1007/s10973-023-12260-8

Sintering of metallic diamond alloy powders

Thomaz Augusto Guisard Restivo[1] · Raphael Basilio Pires Nonato[1] · Rossana Rossoni Figueira[1] · Odirlei Amaro Ferreira[1] · Claudio Padovani[1] · Norberto Aranha[1] · Denicesar Baldo[1] · Cecilia Guedes e Silva[2] · Michelangelo Durazzo[2]

Received: 20 December 2022 / Accepted: 6 May 2023 / Published online: 1 June 2023

Abstract
Metallic diamond (MD) is a new alloy class which hardness was found to surpass any current alloys at more than a twofold factor, up to 2500 HV (kgf mm^{-2}). The alloy design employs simple metallurgical principles at the so-called Lattice Occupancy Project aided by Diamoy 1.0 software. The most important aspect of the alloy project considers the maximization of chromium equivalent values by selecting metallic elements for promoting body-centred cubic structures. Forming these alloys into parts is challenging, whereas powder metallurgy techniques appear as valid processing routes. The work studies the sintering behaviour of MD-4 and 5 alloy powders, being the hardest MD ones. High energy milled powder compacts were sintered in a dilatometer up to 1500 °C for 1 h under Ar-10%H_2 atmosphere. Alloy MD-5 has shown intense shrinkage starting at 1150 °C, contrasting to marginal sintering of alloy MD-4. The latter has undergone transformations from 400 °C with strong expansion, which seems to block most of the sintering retraction at higher temperatures. Alloy powder MD-5 is a good candidate as a raw material for tool parts production by powder metallurgy, which can compete with cemented carbide hard tools.

Keywords Metallic diamond alloys · Hardness · Sintering · Dilatometry

Introduction

Metallic diamond alloys (MD alloys) have been developed by arc melting of several chosen metallic elements to obtain a body-centred cubic material (BCC). These materials show higher hardness than the current types of steels or metallic alloys. MD alloys are formulated including 6 to 9 elements, among which some refractory metals such as Nb, V, Mo and Ti, in addition to Fe, Cr and other metals.

MD alloys are similar to high entropy alloys (HEA) broadly studied worldwide [1–3]. Systematic reviews have been examined hundreds of HEA compositions, mechanical and other useful properties displaying great advancements and superior behaviours. Vickers hardness values of HEAs are usually limited to 950 HV (Kgf mm^{-2}) or 8.8 GPa [4]. Usually, refractory metals take part of the formulations, often including Zr, Hf and W together with other elements [5]. In some cases, HEA alloys present yield strains over 2500 MPa at room temperature and above 1000 MPa at high temperatures. Most of HEA contains Co, Ni and sometimes Mn, which are gammagenic elements and would promote face-centred cubic structures (FCC) [6]. Actually, the common structure found at HEA after alloy elaboration is a mixture of phases such as BCC + FCC and Hexagonal Close-Packed (HCP), as well as intermetallic ones [4, 5, 7]. Some refractory metal bearing HEAs (RHEAs) have been considered as an advantageous alternative for high temperature applications, since ultimate stresses over 400 MPa were measured at 1600 °C [5, 7–9]. The RHEAs are often crystallized in BCC structure, which is harder than FCC or even HCP. The elements selection and structure/ properties simulation of HEAs have been conducted by computation methods such as CALPHAD and DTF first principles, sometimes combined with parametric approaches [5, 10, 11].

In spite of containing several different elements and some refractory ones, metallic diamond alloys are substantially different regarding HEAs or RHEAs materials in some

✉ Thomaz Augusto Guisard Restivo
thomaz@protolab.com.br

[1] University of Sorocaba, Rod. Raposo Tavares Km 92, Sorocaba, SP 18023000, Brazil

[2] IPEN – Nuclear and Energy Research Institute, Av. Lineu Prestes 2242, Sao Paulo 05508000, Brazil

aspects. A new simple alloy design called Lattice Occupancy Alloy Project (LOAP) is the basis for formulating the alloys [12, 13], where a final body-centred cubic (BCC) structure is sought with 9 atomic positions for 9 distinct elements. Besides the normal topological and thermodynamic parameters employed for HEAs [14], such as δ, γ, Ω, VEC, the LOAP project selects those metallic components which give high chromium equivalent sums according to conventional equations [12, 15]. In this sense, Creq total sum is considered as the key parameter for selecting the alloy elements. Therefore, one may choose those alloy elements showing more important Creq coefficients (alphagenic elements), where Mo, V, Nb and Ti match such requirements since their coefficients are rated from 2 to 4. This approach is based on the promotion of the BCC structure and on the expansion of its field of stability, leading to increased metal solubility between each other. It is worthwhile to note that the MD alloys do not employ Co, Ni or other FCC promoter elements showing negative coefficients at Creq equations.

An alternative project design assumes that instead of 9 elements occupying positions in the BCC lattice, the same element can be repeated 3 times. In this case, the new 7-elements alloys have been proven to render the highest hardness results. The alloy project is built using the software Diamoy 1.0, specially designed for selecting the elements and delivering dozens of parameters, allowing to check the assembly of element for the resulting alloy [16, 17].

The typical hardness of the as-cast MD alloys is in the range 900–1100 HV (Vickers), while increasing up to 1900 HV after annealing at 1200 °C, and above 2500 HV for carburized samples at 1200 °C, exceeding the corresponding values for HEAs and any other alloy types [4].

Fabrication of MD alloys can be an issue due to cutting, machining and forming operations, which require SiC and diamond tools along with very high loads. Therefore, powder metallurgy techniques are envisioned in order to fabricate parts.

Liquid phase sintering (LPS) phenomena have been figured out for driving the densification of green bodies. Copper additive was chosen since it melts during the sintering cycle and deliver a liquid phase, which can bring the particles closer through capillarity forces for aiding the shrinkage, as well as such liquid can dissolve some species, therefore increasing the diffusion rates.

The article studies the sinterability of two powder compositions obtained from cast alloys for initially validate the powder metallurgy route.

Experimental

Two 7-elements alloys, MD-4 and 5, were formulated from individual metal powders with 99.5 + % purity of each element, mixed and pressed into 23 mm diameter die, afterward being plasma melted over a copper tray under 0.2 MPa high purity flowing argon and poured into a copper mold:

- MD-4 alloy: $FeCr_3MoNbTaTiV$
- MD-5 alloy: $Fe_3CrMoNbTaTiV$

The resulting ingots were powdered by mechanical means including hammering and pressing into a 50 mm diameter die to avoid contaminations due to friction. Afterwards, the particles underwent high energy milling (MA) at a shaker mill (19 Hz) for 20 min with SAE52100 steel spheres with diameters of 5 and 8 mm in a mass ratio balls to powder of 7:1. The resulting powder was collected under a 200 µm sieve. The powder was pressed in a 3.5 mm diameter cylindrical die at 400 MPa and the pellets were placed in a dilatometer (SETARAM Setsys TMA 18) under 2 g load. The employed atmosphere was 50 mL min^{-1} dynamic Ar-10%H_2, and the heating rate was 10 °C min^{-1} up to 1500 °C, with a dwelling time of 1 h. This set of parameters is suitable for detecting shrinkage trends up to the densification while partial H_2 containing atmosphere is used to assure the pellet is not oxidized during the cycle. The samples were also analysed at a Setaram Setsys Evolution 18 DSC up to 1500 °C with the same heating rate and atmosphere and no holding time. The sample holder, probe and crucibles were made from dense alumina. In an attempt to increase the densification, a sintering promotion additive—3 mass% Cu 3 µm powder—was mixed with MD-5 powder. Copper additive was selected since it has no solubility in most refractory metals found in the alloy formulation, actually being repealed by such metals [18, 19]. In this way, Cu remains as a rather pure liquid phase during all the process and can aid the densification by LPS phenomenon. Some 8 mm diameter MD pellets were also pressed at 400 MPa for sintering at a vertical muffle furnace in the range 1300–1450 °C, under dynamic Ar-4%H_2 atmospheres. Sample powders, casts and sintered pellets were characterized by SEM (Jeol IT200) and XRD (Rigaku Miniflex) for microstructures and phases. Cast and sintered samples were mounted in resin and polished down to 3 µm with diamond paste. Loose powder samples were dispersed over an adhesive carbon tape for observation at SEM. The SEM accelerating voltage employed was 20 kV, with a mixed image of backscattering/secondary electrons (BSE/SE) with 75% BSE. In addition to cast samples, sintered pellets were crushed to powder for XRD analysis with Cu K-alpha radiation from 20° to 120° 2-theta degree, 0.02° step size and 2° min^{-1} scanning time.

Table 1 Sintering results of pressed pellets under different conditions in % of theoretical density %TD; MD-4 and MD-5 TD is 9.65 and 8.96 g cm^{-3} measured by He pycnometry

Sample	condition	Green %TD	Sintered %TD	Δ%TD
MD-4	Dilatometer 1500 °C/1 h	57.43	58.24	0.81
MD-4	Furnace 1450 °C/3 h	61.36	73.93	12.57
MD-4	Furnace 1400 °C/3 h	56.34	63.21	6.87
MD-5	Dilatometer 1500 °C/1 h	64.46	88.10	23.64
MD-5	Furnace 1450 °C/3 h	58.20	82.17	23.97
MD-5	Furnace 1400 °C/3 h	62.03	85.75	23.71
MD-5 + 3% Cu	Dilatometer 1500 °C/1 h	65.52	86.41	20.89
MD-5 + 3% Cu	Furnace 1450 °C/3 h	60.92	89.79	28.87
MD-5 + 3% Cu	Furnace 1400 °C/3 h	62.94	86.06	23.12

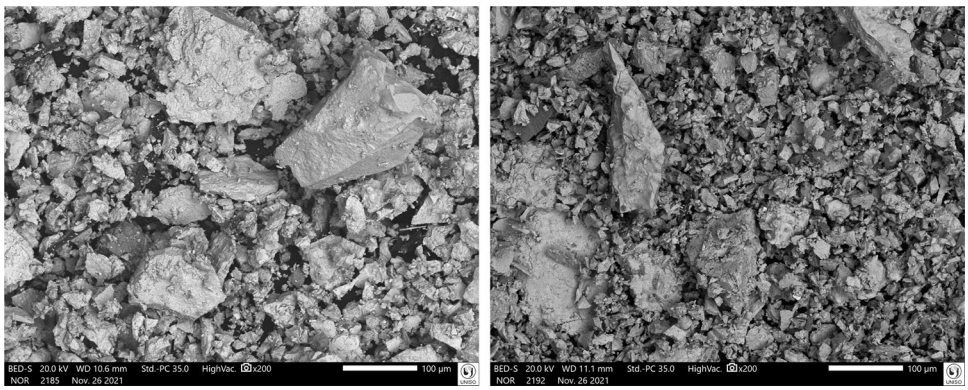

Fig. 1 SEM BSE images of MD-4 (left) and MD-5 alloy powders

Results and discussion

Sintered geometric final densities are shown in Table 1 for several run conditions at the dilatometer and sintering furnace. MD-5 alloy powders attain higher sintered densities while MD-4 alloy final densities are smaller in all conditions. The resulted small final density of MD-4 compact at the dilatometer can be related to higher H_2 content and oxygen absence in the controlled atmosphere at the sample chamber during sintering, being such conditions not fully found in the sintering furnace. This result suggests there is some effect of hydrogen on preventing sintering due to metal hydriding and elements recombination at high temperatures to form some phases acting as barriers. Furthermore, the effect of sintering temperature is more critical for MD-4 powder compacts, leading to a smaller final density, for instance, comparing the results at 1450 °C with 1400 °C in the furnace. The difference in terms of % TD (theoretical density) between sintered and green density is strongly affected by the dwelling time at sintering temperature. The admixture of Cu additive has a further influence on increasing the final density with a maximum Δ%TD of 28.87%, which suggests the LPS is an important sintering mechanism. However, even the undoped MD-5 powder compacts sinter to similar densities, indicating the LPS phenomena may occur within the alloy itself.

Figure 1 shows the back scattered electron SEM-BSE images of both powders, where it can be seen the MD-4 powder is somewhat coarser than MD-5 one after 20 min MA milling, leading to smaller green density for the former. According to previous results [12, 13], MD-4 is slightly harder than MD-5; hence the powder is more difficult to be refined by milling. There is little contrast in SEM-BSE powder images, indicating the powder particles are rather homogeneous.

Figure 2 shows the retraction profiles up to 1500 °C for both alloys together with the DSC curves. MD-4 alloy has shown marginal shrinkage, while MD-5 alloy has good sinterability up to 1500 °C. The shrinkage rate of MD-5 attains high values of -3% min^{-1} (− 85 µm min^{-1}) at 1490 °C. It can be seen at DSC curves there is a melting peak for MD-5 powder at 1419 °C, followed by a solidification one at 1382 °C during cooling. Such peaks correspond to liquid

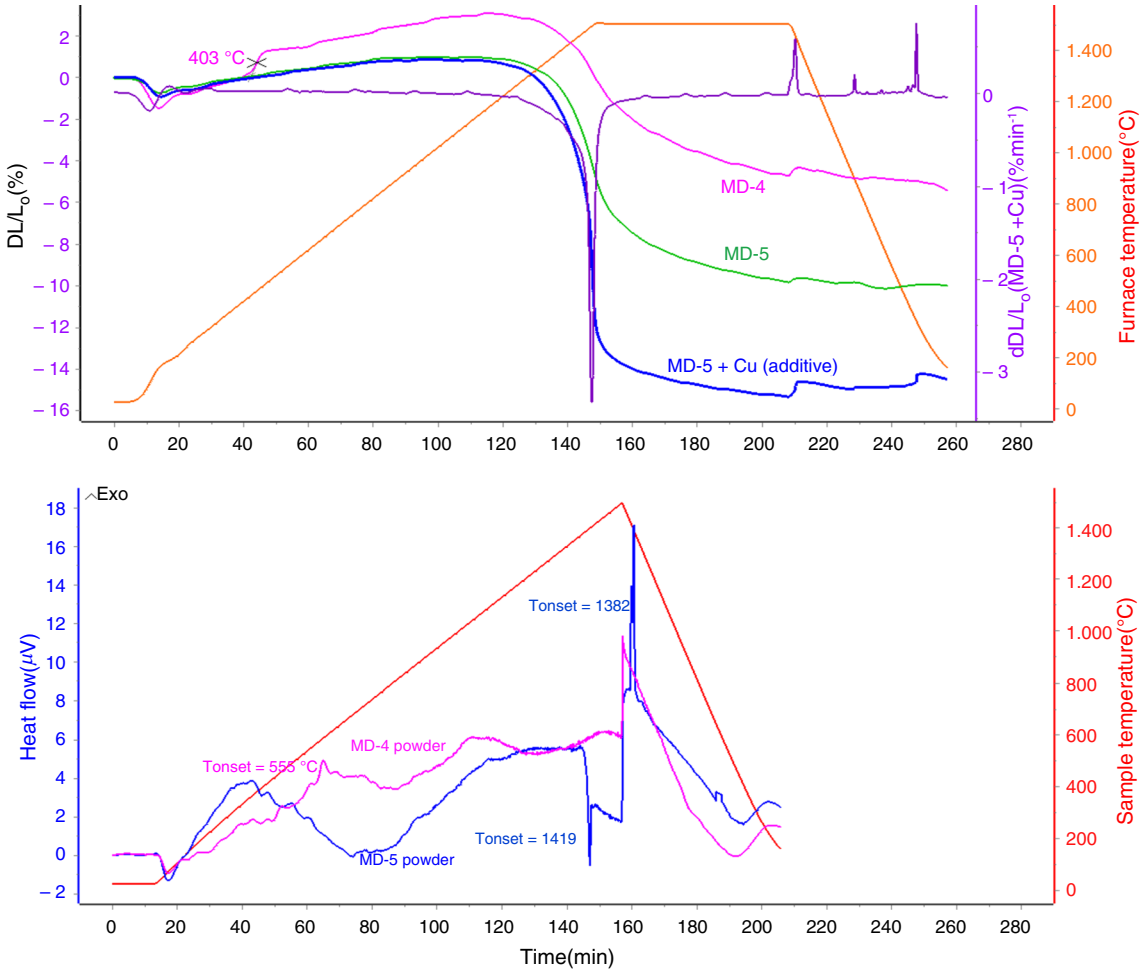

Fig. 2 Dilatometric profiles up to 1500 °C under Ar-10%H2; pellets from powdered MD-4 alloy and MD-5 alloy with and without 3% Cu additive; retraction rate is also shown for MD-5 + Cu; bellow: DSC curves for MD-4 and 5 powders

phase formation already found in the alloy, which explain the best sinterability of MD-5 powder, even without Cu additive. On the other side, MD-4 has no clear melting peak, but conversely an endothermic set of peaks indicates some phases are forming before 558 °C, leading to a strong expansion from 403 °C and sintering blockage thereafter.

Sintering microstructures observed at SEM in Fig. 3 confirm the higher density of MD-5 compared to MD-4, especially when doped with Cu. EDS maps for alloy elements and additive were recorded and displayed for Ti and Cu, being the other elements distributed homogeneously. Black droplets or nodules, detected as metallic Ti, sometimes with low V, are present in the microstructure, which seems to be precipitated from the alloy. Those dark fields were not associated with C, O or N at the EDS maps, which were not detected in significant amounts. As depicted, raw materials for preparation of alloys are high purity metals cast under high argon pressure. Dark Ti nodules morphology is clearly originated from a molten phase, say, droplet-like features and rounded surfaces. Ti or Ti-V solid solution shows melting temperatures above 1600 °C [20–22], therefore suggesting some other minor element is taking part at such phase to render a eutectic liquid constituent at sintering temperatures. Cu additive has been flowed and coalesced to triple points of sintered particles, playing its role as LPS promoter.

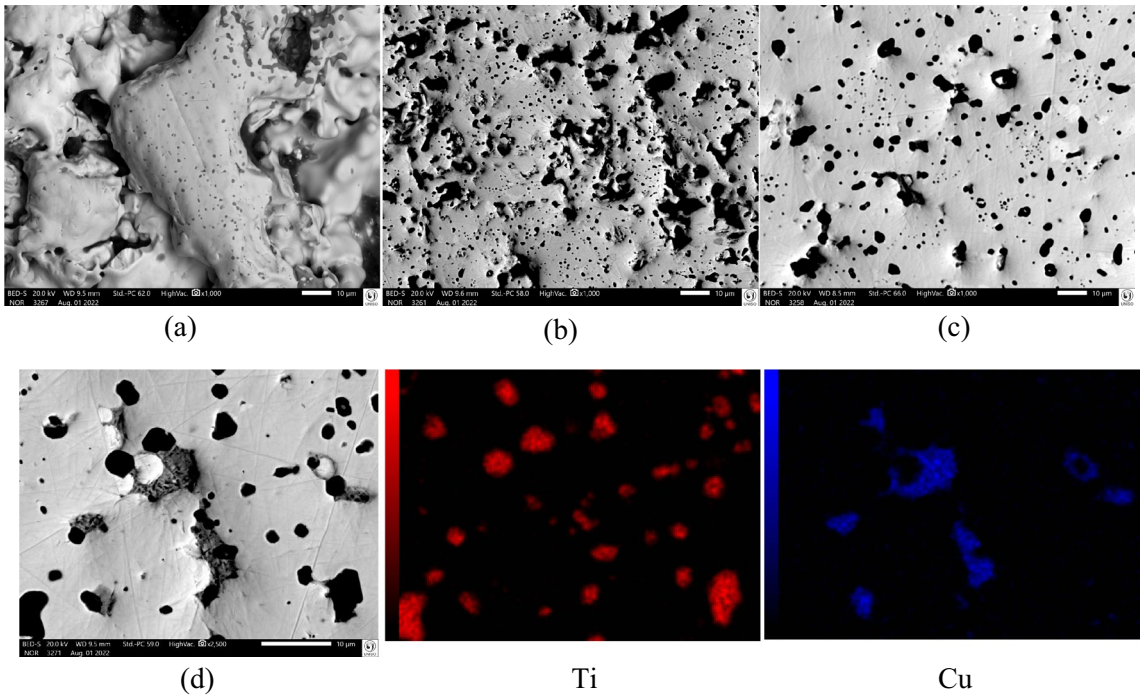

Fig. 3 SEM images of 1500 °C sintered powder: **a** MD-4; **b** MD-5; **c** MD-5 + 3% Cu and **d** MD-5 + 3% Cu with corresponding Ti and Cu EDS maps

X-ray diffraction profiles of MD-4 and MD-5 alloys were grouped for as-cast, MA milled powder and 1400 °C sintered pellet in Fig. 4. The as-cast XRD profiles are more crystalline while the MA powders tend to be amorphous, as expected after strong particles refining and deformation, which was partially recovered by the sintering process. All peaks could be indexed to BCC cubic systems, named as α, β, δ and ε, starting from the strongest intensities at the diffractograms for the as-cast and sintered alloy. Both alloys show some phases which were split in other ones, earlier after the milling process, as well as new phases have appeared. The main α and β phases were shifted from their original reflection angles, indicating that some metal atom constituents have diffused from the original alloys during processing. The sintered XRD profile of MD-4 alloy is complex, where 4 different main phases could be indexed besides other minor phases. This result can be related to dilatometry and DSC events found for the MD-4 alloy, which can lead to retraction blockage during the process by interposing new forming phases and slowing the diffusion of species. Conversely, MD-5 XRD profiles are less complex and more crystalline, even in the milled powder form. MD-5 main α-phase peak intensity seen at as-cast sample was conserved up to the sintered profile and even has increased, suggesting there is a crystallinity enhancement during sintering at high temperature. Such results are consistent with the good sintering behaviour of MD-5 powder compacts. Some copper peaks were also identified in the sintered MD-5 sample with small shifting regarding the elemental file (JCPDF 04-0836), indicating this metal has very low solubility in the alloy and acts as LPS additive to promote the densification, in agreement with the earlier assumptions.

The compilation of hardness and fracture toughness based on Palmkvist radial crack lengths [23] is shown in Table 2 for cast ingots and sintered powder compacts. The hardness of high-temperature MD-5 sintered pellets, as well as the fracture toughness, approaches the respective as-cast properties. Actually, it seems there are some gains on hardness level for sintered MD-5 alloy, reaching a maximum value of 1117 HV (10.95 GPa). Crack lengths were not revealed at some low-density pellets such as MD-4 and MD-5 sintered at 1400 °C due to the excess of porosity, where low hardnesses were measured as well. The results also confirm that Cu additive does not affect the hardness values of sintered MD-5 alloy pellet since the metal flows to triple points during sintering, being isolated.

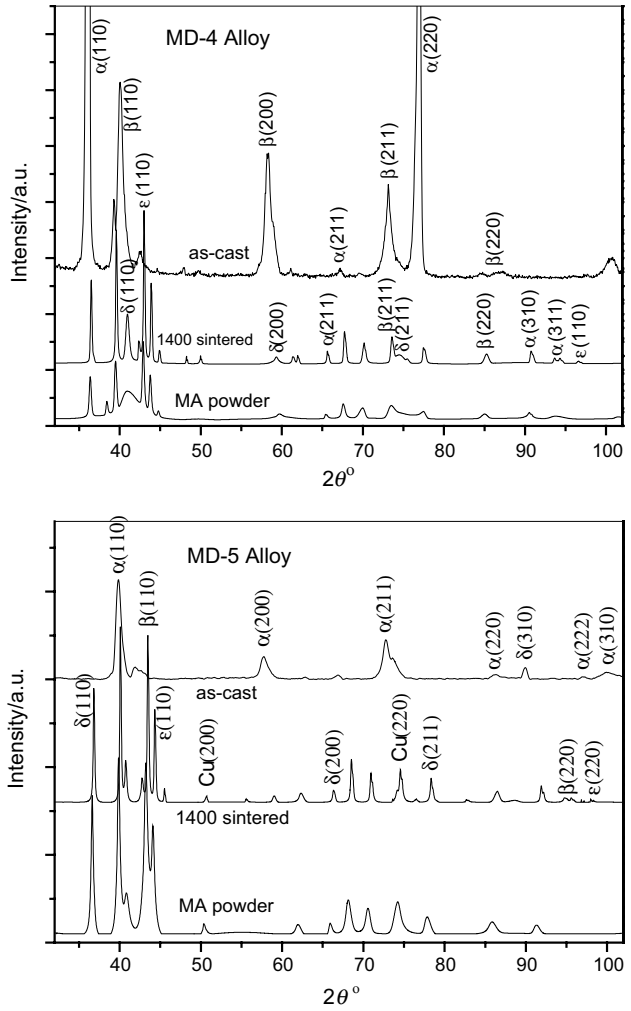

Fig. 4 XRD profiles of MD-4 and MD-5 for as-cast, powder and sintered conditions

Table 2 Hardness and fracture toughness ranges of cast and sintered pellets

Sample	HV/1 kg range/kgf mm^{-2}	K1C/MPa m$^{1/2}$
MD-4 as-cast ingot	876–921	7.8–10.2
MD-5 as-cast ingot	867–997	7.7–8.1
MD-4 sintered 1400 °C/3 h	203–551	–
MD-5 sintered 1400 °C/3 h	398–683	–
MD-5 + 3% Cu sintered 1400 °C/3 h	727–980	7.2–8.2
MD-5 + 3% Cu sintered 1450 °C/3 h	867–1117	7.4–8.2

Conclusions

New metallic diamond alloys were for the first time cast and turned into powder form, followed by consolidation through sintering. MD-4 alloy has shown earlier expansion and a sintering barrier during early heating leading to low pellet shrinkage. On the other side, MD-5 alloy is promptly sintered to high densities. Copper additive rated at 3 mass% is effective in promoting sintering by LPS, leading to higher densities while not affecting the measured final hardness. Moreover, a liquid phase seems to form in MD-5 powder alloy from itself. XRD analysis demonstrates the system is more complex for MD-4 alloy and derived materials, where initial 1 to 3 BCC phases were split into 4 or more ones, together with shifting of peak positions. MD-5 is more crystalline and has shown some phases stability, accordingly to the results.

The new Metallic Diamond material MD-5 is suitable for powder metallurgy process manufacturing of parts with good properties.

Acknowledgements The authors acknowledge the research councils CNPq (proj. 408406/2021-6), CatalisaICT Sebrae (proj. 29083*128) and FAPESP (proj. 2020/09736-3) for the financial support.

References

1. Gao MC, Yeh JW, Liaw PK, Zhang Y. High-entropy alloys. Fundamentals and applications. Switzerland: Springer International Publishing; 2016.
2. Miracle DB, Senkov ON. A critical review of high entropy alloys and related concepts. Acta Mater. 2017;122:448–511.
3. George EP, Raabe D, Ritchie RO. High-entropy alloys. Nat Rev Mater. 2019;4:515–34.
4. Gorsse S, et al. Database on the mechanical properties of high entropy alloys and complex concentrated alloys. Data Brief. 2018;21:2664–78.
5. Senkov ON, et al. Development and exploration of refractory high entropy alloys—a review. J Mater Res. 2018;33(19):3092–128.
6. Brandi SD, Schön CG. A Thermodynamic study of a constitutional diagram for duplex stainless steels. J Phase Equilib Diffus. 2017;38:268–75.
7. Chen J, et al. A review on fundamental of high entropy alloys with promising high–temperature properties. J Alloy Compd. 2018;760:15–30.
8. Wan Y, et al. WReTaMo refractory high-entropy alloy with high strength at 1600 °C. Adv Eng Mater. 2022;24:2100765.
9. Chen S, Qi C, Liu J, Zhang J, Wu Y. Recent advances in W-containing refractory high-entropy alloys—an overview. Entropy. 2022;24(11):1553.
10. Guruvidyathri K, et al. Topologically close-packed phase formation in high entropy alloys: a review of calphad and experimental results. JOM. 2017;69:11.
11. Ruixuan L, et al. High-throughput calculations for high-entropy alloys: a brief review. Front Mater. 2020;7:290.
12. Restivo TAG, Restivo GMG. Development of ultra-hard multicomponent alloys. J Mater Res. 2021;36:1316–27.
13. Restivo TAG. Ligas metálicas multi-elementares de extrema dureza tratáveis por processos térmicos e químicos e respectivo projeto, preparação e tratamento. Patent BR102019025461-0, INPI, 02/12/2019.
14. Hu Q, et al. Parametric study of amorphous high-entropy alloys formation from two new perspectives: atomic radius modification

and crystalline structure of alloying elements. Sci Rep. 2017. https://doi.org/10.1038/srep39917.
15. Ryu SH, Yu J. A new equation for the Cr equivalent in 9 to 12 pct Cr steels. Met and Mat Trans A. 1998;29A:1573–8.
16. Nonato RBP, Restivo TAG. Software solution for ultra-hard metal alloy design. Engenharia, Gestão e Inovação, vol. 3. 1st ed. Belo Horizonte: Editora Poisson; 2022. p. 179–87.
17. Nonato R, Restivo T, et al. Software creation for ultra-hard metal alloy design. In: Ulhôa JLR, et al., editors. Engenharia: a máquina que constrói o futuro, vol. 9. 1st ed. Piracanjuba: Editora Conhecimento Livre; 2022. p. 168–81.
18. Restivo TAG, Castanho SRHM, Tenorio JAS. TG/DTA-MS evaluation of methane cracking and coking on doped nickel-zirconia based cermets. J Therm Anal Calorim. 2014;118:75–81.
19. Restivo TAG, Castanho SRHM. Cu-Ni-YSZ anodes for solid oxide fuel cell by mechanical alloying processing. Int J Mater Res. 2010;101:128–32.
20. Bermingham MJ, et al. Microstucture of cast titanium alloys. Mater Forum. 2007;31:84–9.
21. Ghosh G. Thermodynamic and kinetic modeling of the Cr-Ti-V system. J Phase Equilib. 2002;23(4):310–28.
22. Yang Y, Mao H, Chen H-L, Selleby M. An assessment of the Ti-V-O system. J Alloy Compd. 2017;722:365–74.
23. Hanyaloglu SC, Aksakal B, Bolton JD. Production and indentation analysis of WC/Fe–Mn as an alternative to cobalt-bonded hardmetals. Mater Charact. 2001;47:315–22.